Catalysis Communications 11 (2010) 973–976

Contents lists available at ScienceDirect

Catalysis Communications

journal homepage: www.elsevier.com/locate/catcom

Synthesis of a stable and porous Co–B nanoparticle catalyst for selective hydrogenation of cinnamaldehyde to cinnamic alcohol

Zhijie Wu, Jingshi Zhao, Minghui Zhang *, Wei Li, Keyi Tao

Institute of New Catalytic Materials Science, Department of Material Chemistry, College of Chemistry, and Key Laboratory of Advanced Energy Materials Chemistry (MOE), Nankai University, Tianjin, 300071, China

ARTICLE INFO

Article history:
Received 9 March 2010
Received in revised form 20 April 2010
Accepted 22 April 2010
Available online 12 May 2010

Keywords:
Co–B
Cinnamaldehyde
Hydrogenation
Nanoparticles
Electroless plating

ABSTRACT

The Co–B nanoparticle catalyst supported on TiO_2 for the selective hydrogenation of cinnamaldehyde to cinnamic alcohol was prepared by a modified electroless plating method. The as-prepared catalyst was characterized by X-ray diffraction and transmission electron microscope. The results showed that porous Co–B nanoparticles were distributed narrowly (40–45 nm) over the support. Compared with the Co–B nanoparticles prepared by chemical reduction of Co^{2+} ions with borohydride, the as-resulted Co–B nanoparticles were stable to be stored in air, and exhibited higher activity and selectivity of cinnamic alcohol in cinnamaldehyde hydrogenation.

1. Introduction

Selective hydrogenation of α, β-unsaturated aldehydes to unsaturated alcohols is a critical step in the industrial production of chemicals, such as perfumes, flavorings and pharmaceuticals [1]. Because the thermodynamics favor the hydrogenation of the C=C bonds in α, β-unsaturated aldehydes, more attention has been focused on promoting the selectivity of unsaturated alcohol [2]. The selective hydrogenation of cinnamaldehyde (CAL) to cinnamic alcohol (CMO) is frequently reported as a probe reaction to sieve catalysts [3]. Besides the noble metals (Pt, Ir, and Os), transition metal Co exhibits high hydrogenation activity and CMO selectivity. So far, Co-contained catalysts are mostly used for the liquid hydrogenation. Recently, two groups reported that the amorphous Co–B nanoparticles prepared by chemical reduction of Co^{2+} ions with borohydride exhibit high activity and selectivity as noble metals in the CMA hydrogenation [4–7]. The Co–B nanoparticles are regarded as a kind of metal-metalloid amorphous alloy particles, in which the coordination-unsaturated and electron-rich Co element benefits to activate the C=O bond prior to C=C bond [1–8].

The Co–B nanoparticles prepared by the chemical reduction method are sensitive to air or water, and their activities decrease after storing and reaction because its surface is easily covered by boron oxides or formed into metal oxides or metal hydroxides [9,10]. This inhibits the further industrial application of such catalysts. In fact, it is interesting to find that such amorphous metal-metalloid materials are also widely used in corrosion-resistant science, just only turning the preparation method to electroless plating technique [11]. For the electroless plating, the metalloid elements (B and P) are selectively located at the defect of the plated film to protect the corrosion of metal crystals [11–14]. The films are composed by various metal clusters and metal-metalloid clusters, resulting in amorphous structure with short-range order and long-range disorder. In our previous work, we have developed the electroless plating method to synthesize supported amorphous Ni–B nanoparticles for hydrogenation [15–18]. The Ni–B nanoparticles showed high activity and selectivity owing to the modification of structure and electronic properties by B element, which is the same as those particles prepared by chemical reduction, and exhibited higher stability for storing and recycling [15,16,19,20]. Here, to get a stable, active and selective Co–B metal catalyst for CMA hydrogenation, a modified electroless plating method was developed to synthesize amorphous Co–B catalyst. Its structure and catalytic performance were studied in comparison with Co–B nanoparticles prepared by impregnation–reduction method.

2. Experimental

2.1. Catalyst preparation

The Co–B nanoparticle catalyst supported on TiO_2 was prepared by a modified electroless plating method, and the silver metal was used to activate the plating solution [15–18]. The Ag/TiO_2 was prepared in the light of ref. [15]. For the synthesis of $Co–B/TiO_2$ catalyst, the Ag/TiO_2 was added to a Co–B plating solution containing 9 g/L

* Corresponding author. Tel.: +86 22 2350 7730; fax: +86 22 2350 7730.
E-mail address: zhangmh@nankai.edu.cn (M. Zhang).

1566-7367/$ – see front matter © 2010 Elsevier B.V. All rights reserved.
doi:10.1016/j.catcom.2010.04.018

$CoCl_2 \cdot 6H_2O$, 50 g/L $Na_2C_4H_4O_6 \cdot 2H_2O$, 2 g/L $Na_2B_4O_7 \cdot 10H_2O$, 2 g/L NH_4Cl, 6 g/L KBH_4, and NaOH for adjusting the pH = 13. The plating occurred at 45 °C for 30 min. The resulted black product (denoted as Co–B(EP)/TiO_2) was washed with distilled water by centrifugation thoroughly to obtain pH = 7, then washed with ethanol to remove the water. The unsupported Co–B catalyst was also prepared by adding 2.0 mL 0.1 mol/L $AgNO_3$ solution to 200 mL Co–B plating solution. The resulted supported and unsupported catalysts were dried at 80 °C in oven, and stored in air at ambient conditions. For comparison, a conventional Co–B(IR)/TiO_2 catalyst containing 15 wt.% Co was prepared by impregnation–reduction method with the same mole ratios of borohydride/Co = 3, and was stored in ethanol [21]. The Co/TiO_2 catalyst was also prepared by wetness impregnation of TiO_2 with $Co(NO_3)_2$ solution and reduced with hydrogen gas at 400 °C.

2.2. Characterization

The chemical composition of samples was analyzed by inductively coupled plasma atomic emission spectrometry (ICP-AES) on an IRIS Intrepid Spectrometer. X-ray diffraction patterns were collected on the Rigaku D/max-2500 diffractometer by using Ni-filtered Cu Kα radiation (λ = 1.5418 Å) at a scan rate of 2°/min. Transmission electron microscopy (TEM) was carried out on a FEI Tecnai G2 high resolution transmission electron microscope. The active surface area (S_{Co}) was measured by hydrogen chemisorptions on a Quantachrome CHEMBET 3000 TPR/TPD unit by assuming H/Co(s) = 1 [22].

2.3. Catalyst testing

The hydrogenation of cinnamaldehyde (CAL) to cinnamyl alcohol (CMO) was performed in 250 mL stainless steel autoclave which contained 0.1 g metal catalyst, 20.0 mL CAL and 100.0 mL ethanol. The experiment was carried out at 100 °C and 1.5 MPa of hydrogen pressure with stirring at 800 rpm for 3 h The possibility of diffusion limitation during the catalytic tests was investigated as the following procedures described elsewhere [16]. Experiments were carried out at different stirring velocities in the range of 100–1000 rpm. The constancy of the activity and selectivity above 600 rpm ensured that external diffusion limitation was absent at the rotation speed selected. The catalytic activity of the inner wall of the reactor could be neglected, as found by experiments. Blank experiment with Ag/TiO_2 catalyst was carried, and no conversion of CAL was detected. The products were analyzed by a gas chromatograph equipped with a flame ionization detector.

3. Results and discussion

3.1. Characterization of catalysts

Fig. 1 shows the XRD patterns of unsupported and supported Co–B samples. Two broad and featureless peaks at 2θ = 22° and 45° are observed in the XRD pattern of unsupported Co–B sample. The peak at 22° corresponds to the presence of amorphous boron oxides, and the peak around 2θ = 45° indicates the amorphous structure of Co–B nanoparticles. The supported Co–B(EP)/TiO_2 catalyst exhibits only diffraction lines corresponding to anatase TiO_2. It is the result of high dispersion of Co–B particles on the support and the weak diffraction signal of amorphous Co–B [15]. A homogeneous distribution of Co–B nanoparticles is observed in the TEM image of the Co–B(EP)/TiO_2 sample (Fig. 2). Co–B nanoparticles of 40–45 nm are present in a flower-like shape, suggesting the porous structure of Ni–B particles, in which the pores occur from the diffusion of hydrogen during the precipitation of Co clusters on active metal nuclei [17,18]. The amorphous structure of Co–B nanoparticles is also confirmed by the selected area electron diffraction (SAED) (inset of Fig. 2), as no diffraction spots or rings corresponding to crystalline Co or cobalt boride are observed.

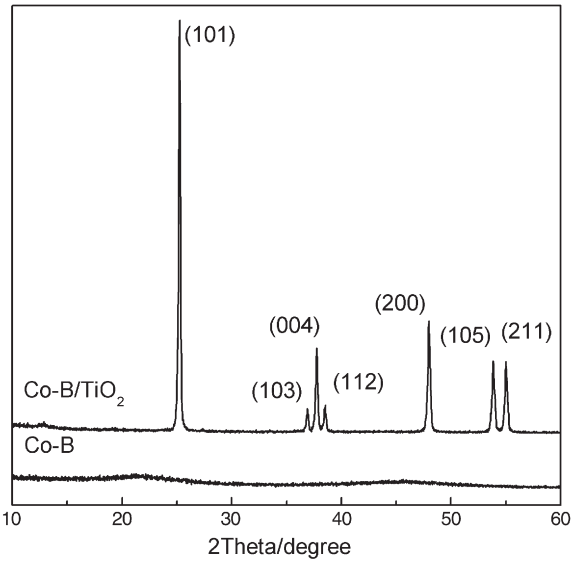

Fig. 1. XRD patterns of unsupported and supported Co–B catalysts.

The supported Co-based catalysts with similar Co loading were prepared by electroless plating and impregnation–reduction methods, and their detail compositions and properties are listed in Table 1. The unsupported Co–B nanoparticles prepared from chemical reduction with borohydride usually show in solid sphere shape [6,7]. The corresponding supported Co–B nanoparticles have smaller particle size and high dispersion. But it is inevitable that some parts of Co–B nanoparticles are aggregated in an unsupported form [15], and some parts of Co metals are present in oxidation states [23], which will reduce the metallic active sites on the Co–B(IR)/TiO_2 catalysts. We note that the Co–B films prepared by electroless plating show excellent anti-corrosion to water and air [11]. Although the Co–B(EP)/TiO_2 has lower Co loading than Co–B(IR)/TiO_2, the Co–B(EP)/TiO_2 catalyst exhibits a higher active metal surface area (S_{Co}).

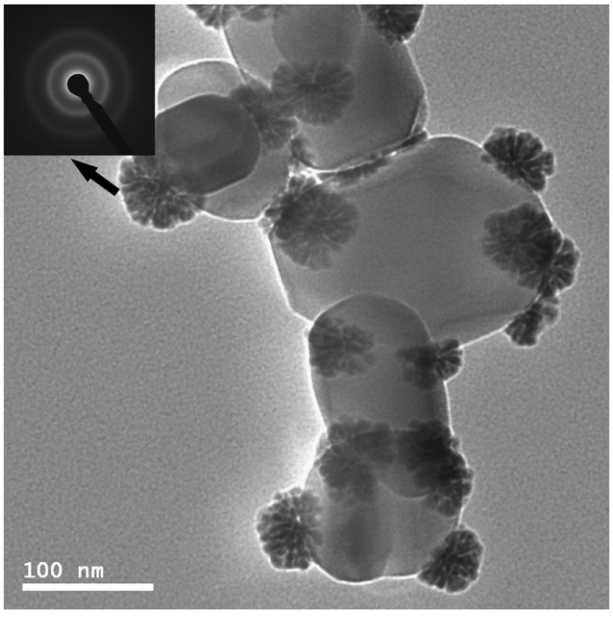

Fig. 2. TEM image of Co–B(EP)/TiO_2 catalyst.

Table 1
Chemical compositions and catalytic properties of catalysts.

Samples	Co loading (wt.%)	S_{BET} (m^2/g)	S_{Co} (m^2/g_{Co})[a]	Composition (%)	TOF (mol $mol^{-1}s^{-1}$)[b]	Conversion (%)	Selectivities[c]			
							CMO	HCAL	HCMO	CEE
Co–B(EP)/TiO_2	13.9	42.5	15.7	$Co_{52.1}B_{47.9}$	0.27	98.0	99.8	0	0.2	0
Co–B(IR)/TiO_2	15.0	37.2	7.5	$Co_{68.7}B_{31.3}$	0.24	40.9	68.2	20.1	8.9	2.8
Co–B(IR)/TiO_2[d]	15.0	36.7	0.5	$Co_{68.7}B_{31.3}$	0.017	0.2	72.1	22.1	5.2	0.6
Co/TiO_2	15.0	–	2.8	–	0.054	3.5	58.8	31.4	7.5	2.3
Ag/TiO_2	0.2	24.3	0	–	–	<0.1	–	–	–	–
Raney Ni	–	–	54.1[e]	–	0.079	100	23.2	65.7	11.1	0

[a] The S_{Co} was measured by the H_2 chemisorptions, which were performed by using a dynamic pulse method. The catalyst was treated by an Ar stream at 200 °C for 1.0 h firstly, which was well below its crystallization temperature.
[b] Reaction turnover frequency which is defined as mole of reactant converted per mol of surface metal atom per second.
[c] Hydrocinnamaldehyde: HCAL; cinnamyl alcohol: CMO; hydrocinnamyl alcohol: HCMO; and cinnamyl ethyl ether (C_6H_5CH $CH–CH_2–O–C_2H_5$): CEE.
[d] The catalyst was stored in air for 24 h.
[e] The active surface area of nickel.

3.2. Activity and stability of catalysts

Table 1 summarizes the physical and catalytic properties of Co catalysts. Blank experiment indicated that Ag/TiO_2 precursor has a negligible effect on the reaction. After the deposition of Co–B nanoparticles on Ag/TiO_2 supports, higher surface area was detected. It is obvious that the higher the surface area of active metal (S_{Co}), the higher the turnover frequency (TOF) and conversion in CAL hydrogenation, suggesting that the activity of Co catalyst is dependent on the S_{Co}. The low S_{Co} value of Co/TiO_2 should be ascribed to the sintering of Co during H_2 reduction because of the small surface area of TiO_2 and high metal loading. The porous Raney Ni catalyst presents high S_{Ni} value, and exhibits the highest conversion when the same amount of metal was used in hydrogenation. However, the amorphous Co–B exhibits higher intrinsic activity than Raney Ni catalyst and crystallite Co catalysts. Deng et al. point that the unique short-range ordering but long-range disordering structure of the amorphous alloy is responsible for its excellent activity and selectivity in many hydrogenation reactions [21]. For Co–B nanoparticles, the Co active site has a stronger synergistic effect between each other and is more highly unsaturated than metal Co, which increases the activity of Co atoms [3]. Thus, the amorphous Co–B shows high activity for hydrogenation of CAL. Table 1 showed that the main products were hydrocinnamaldehyde (HCAL), cinnamyl alcohol (CMO), and hydrocinnamyl alcohol (HCMO), and a little amount of cinnamyl ethyl ether (CEE, C_6H_5CH $CH–CH_2–O–C_2H_5$). The HCMO comes from the further hydrogenation of HCAL and CMO, and the CEE is ascribed to the reaction of CMO with ethanol or the direct reaction of CAL and ethanol with H_2 [24–26]. The Raney Ni catalyst shows the high selectivity toward C=C bond hydrogenation to hydrocinnamaldehyde (HCMA), but Co-based catalysts exhibit much higher selectivity of CMO [2]. The amorphous Co–B nanoparticle catalyst shows a higher selectivity of CMO than crystalline Co catalyst. For the amorphous Co–B nanoparticles, some electrons partially transfer from B to Co, making Co electron-enriched and B electron-deficient in the Co–B nanoparticles [3–6]. The electron-deficient B enhances the total adsorption strength of C=O group on Co–B, and the adsorption of hydrogen increases on the electron-enriched Co active sites [3]. Both Co–B/TiO_2 catalysts show higher activity and selectivity than Co/TiO_2. For the Co–B(EP)/TiO_2, the high S_{Co} and B content result in a high TOF and selectivity of CMO (99.8%). Unlike the Co–B(EP)/TiO_2 catalyst stored in air, the Co–B(IR)/TiO_2 exhibits little hydrogenation activity after storing in air for 24 h.

Fig. 3 shows the stability of Co–B/TiO_2 catalyst for the CAL hydrogenation. The Co–B(EP)/TiO_2 catalyst shows stable conversion and selectivity of CMO during five runs. The conversion on Co–B(IR)/TiO_2 catalyst decreases with hydrogenation times, although the selectivity is also stable. In our previous work, we found that amorphous Ni–B nanoparticles prepared by chemical reduction were sensitive to the oxygen, air and solvent (especially for water), and the surface spices of nickel oxide or hydroxide occurred during the storing and reactions [15–19], which agreed with other group's work [10]. In fact, the review paper (ref. [10]) also pointed the similar problem on the Co–B nanoparticles as Ni–B nanoparticles occurred. So, we concluded that the deactivation of Co–B(IR)/TiO_2 catalyst maybe due to the surface changes, such as surface oxidation [10,15]. In short, the Co–B(EP)/TiO_2 catalyst exhibits higher activity and better stability for selective hydrogenation of CAL than Co–B(IR)/TiO_2. Alternatively, the electroless plating provides a simple route to synthesize high active and selective supported Co–B catalyst. In addition, for the electroless plating, some Co^{2+} should be left in the plating solution after plating due to the complexation of Co^{2+} and $Na_2C_4H_4O_6 \cdot 2H_2O$, and the residual Co^{2+} can be recycled for a further electroless plating, which also reduce the cost of preparation.

4. Conclusions

The Co–B nanoparticles supported on TiO_2 were prepared by the electroless plating method. The porous Co–B nanoparticles were

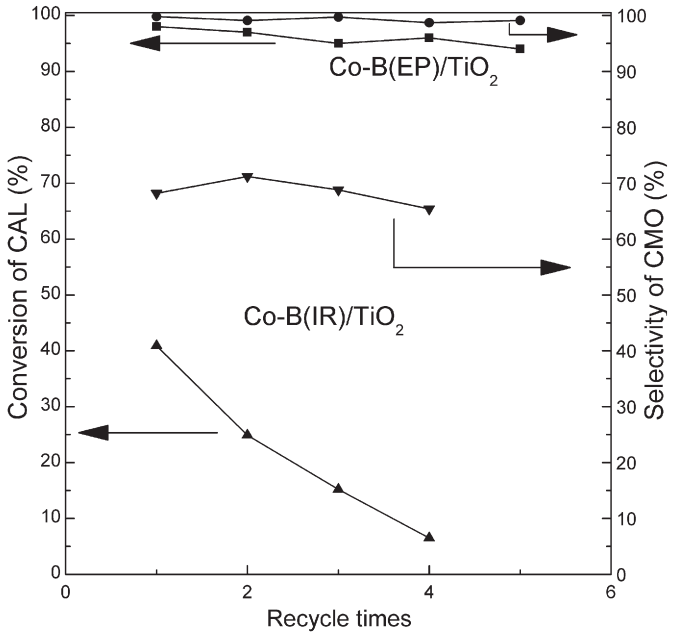

Fig. 3. Catalytic activities and selectivities of Co–B/TiO_2 catalysts in the hydrogenation of CAL.

narrowly distributed with 40–45 nm. The TEM and XRD confirmed the amorphous structure and high dispersion of Co–B nanoparticles. In comparison with Co–B nanoparticles prepared by chemical reduction, the resulted amorphous Co–B(EP)/TiO_2 catalyst showed higher activity and better stability in hydrogenation of CAL. In conclusion, with a high conversion, CAL is highly selectively hydrogenated to CMO over supported Co–B (EP)/TiO_2 catalyst. The present strategy would provide a versatile route of uniform and stable Co nanoparticle catalysts, which would be promising for the design of high activity and selectivity hydrogenation catalysts with high chemical stability.

Acknowledgement

The present work was supported by the Natural Science Foundation of Tianjin (10JCYBJC04400).

References

[1] P. Claus, Top Catal. 5 (1998) 51.
[2] P. Gallezot, D. Richard, Catal. Rev. Sci. Eng. 40 (1998) 81.
[3] H.X. Li, X.F. Chen, M.H. Wang, Y.P. Xu, Appl. Catal. A 225 (2002) 117.
[4] H. Li, J. Liu, S.H. Xie, M.H. Qiao, W.L. Dai, H.X. Li, J. Catal. 259 (2008) 104.
[5] H.X. Li, H. Li, J. Zhang, W.L. Dai, M.H. Qiao, J. Catal. 246 (2007) 301.
[6] D.G. Tong, W. Chu, Y.Y. Luo, X.Y. Ji, Y. He, J. Mol. Catal. A 265 (2007) 195.
[7] D.G. Tong, W. Chu, Y.Y. Luo, C. Hong, X.Y. Ji, J. Mol. Catal. A 269 (2007) 149.
[8] J.V. Wonterghem, S. Morup, C.J.W. Koch, S.W. Charles, S. Well, Nature 322 (1986) 622.
[9] R.C. Wade, D.G. Holah, A.N. Hughes, B.C. Hui, Catal. Rev. Sci. Eng 14 (1976) 211.
[10] G.N. Glavee, K.J. Klabunde, C.M. Sorensen, G.C. Hadjipanayis, Langmuir 9 (1993) 162.
[11] G.O. Mallory, J.B. Hajdu, Electroless Plating: Fundamentals and Applications, American Electroplaters and Surface Finishers Society, Orlando, FL, 1990, p. 1.
[12] X. Yin, L. Hong, B.H. Chen, T.M. Ko, J. Colloid Interface Sci. 262 (2003) 89.
[13] X. Yin, L. Hong, B.H. Chen, J. Phys. Chem. B 108 (2004) 10919.
[14] C.H. Chen, B.H. Chen, L. Hong, Chem. Mater. 18 (2006) 2959.
[15] Z.J. Wu, M.H. Zhang, S.H. Ge, Z.L. Zhang, W. Li, K.Y. Tao, J. Mater. Chem. 15 (2005) 4928.
[16] S.H. Ge, Z.J. Wu, M.H. Zhang, W. Li, K.Y. Tao, Ind. Eng. Chem. Res. 45 (2006) 2229.
[17] Z.J. Wu, S.H. Ge, M.H. Zhang, S.C. Mu, W. Li, K.Y. Tao, J. Phys. Chem. C 111 (2007) 8587.
[18] Z.J. Wu, S.H. Ge, M.H. Zhang, W. Li, K.Y. Tao, J. Colloid Interface Sci. 330 (2009) 359.
[19] Z.J. Wu, M.H. Zhang, W. Li, S.C. Mu, K.Y. Tao, J. Mol. Catal. A 273 (2007) 277.
[20] Z.J. Wu, M.H. Zhang, Z.F. Zhao, W. Li, K.Y. Tao, J. Catal. 256 (2008) 323.
[21] J.F. Deng, H.X. Li, W.J. Wang, Catal. Today 51 (1999) 113.
[22] J.J.F. Scholten, A.P. Pijers, A.M.L. Hustings, Catal. Rev. Sci. Eng. 27 (1985) 151.
[23] K. Molvinger, M. Lopez, J. Court, J. Mol. Catal. A 150 (1999) 267.
[24] Z. Poltarzewski, S. Galvagno, R. Pietropaolo, P. Staiti, J. Catal. 102 (1986) 190.
[25] C. Milone, M.C. Trapani, S. Galvagno, Appl. Catal. A 337 (2008) 163.
[26] K. Nuithitikul, J.M. Winterbottom, Chem. Eng. Sci. 61 (2006) 5944.